

Figure 4.51: Experimental and theoretical data for the derivatives of  $\sigma_1 + \sigma_2$  and the experimental integrated  $\sigma_1 + \sigma_2$  for specimen HomC2 for  $K_I = 0.145 \text{ MPa}\sqrt{\text{m}}$  and  $K_{II} = 0.63 \text{ kPa}\sqrt{\text{m}}$  with crack region masked in blue

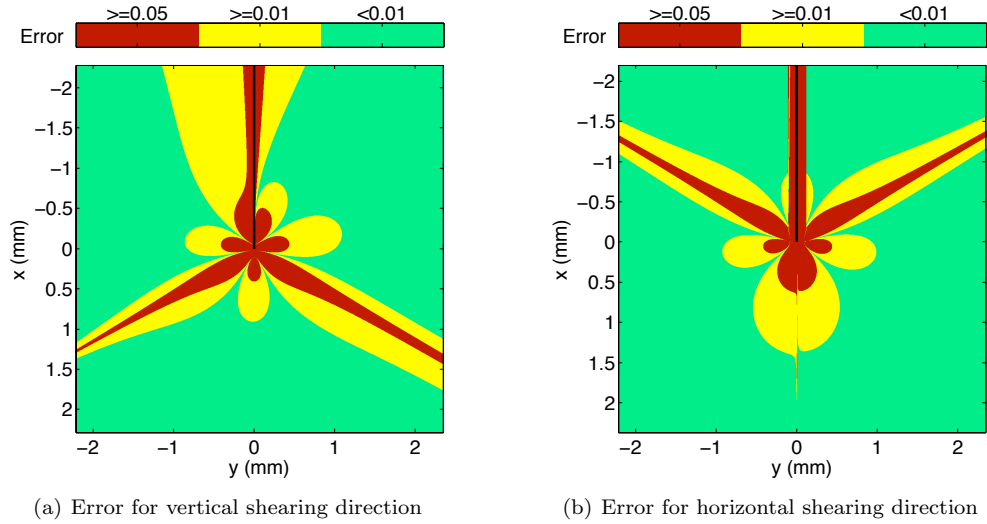


Figure 4.52: Theoretical error for CGS approximating the derivatives of  $K_I = 0.145 \text{ MPa}\sqrt{\text{m}}$  and  $K_{II} = 0.63 \text{ kPa}\sqrt{\text{m}}$  for the  $4.6 \text{ mm} \times 4.6 \text{ mm}$  field of view and lateral shearing distance of  $d_{shear} = 225 \mu\text{m}$  [Crack indicated in black]

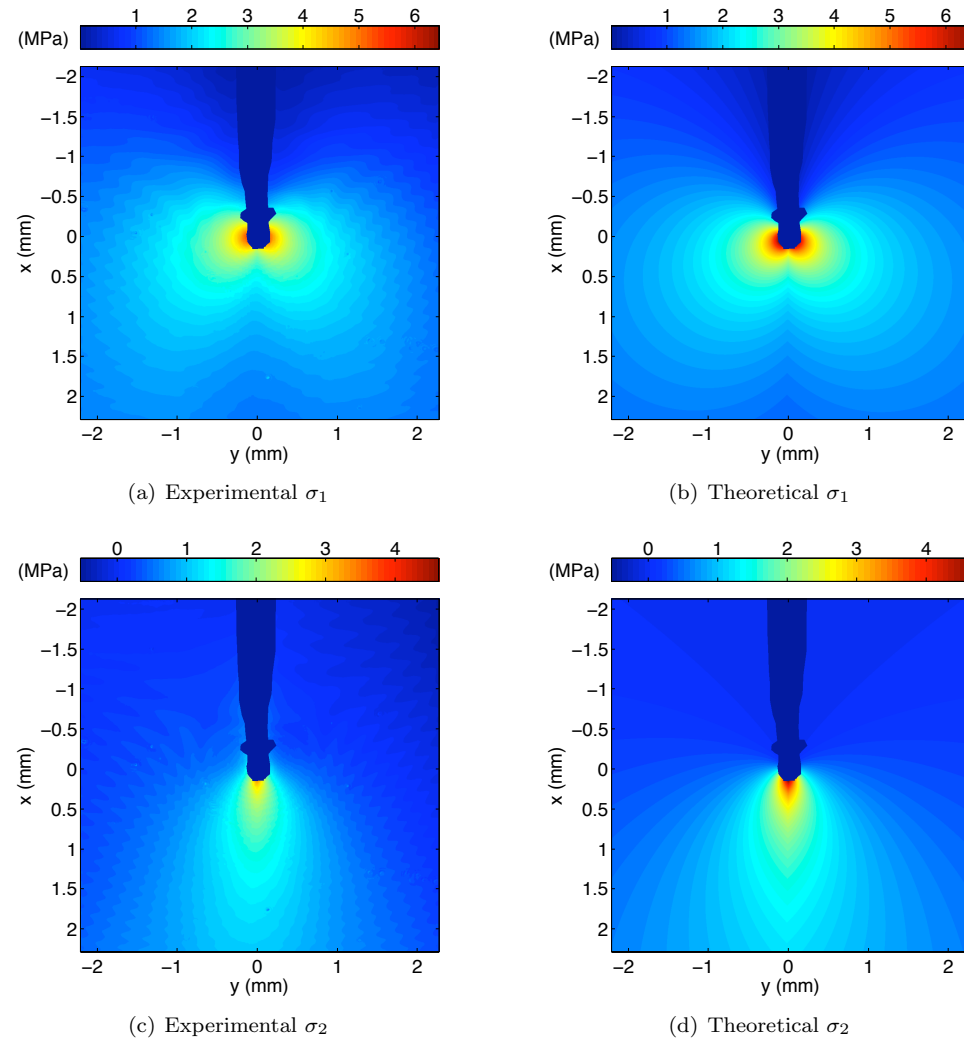


Figure 4.53: Experimental and theoretical data for the principal stresses for specimen HomC2 for  $K_I = 0.145 \text{ MPa}\sqrt{\text{m}}$  and  $K_{II} = 0.63 \text{ kPa}\sqrt{\text{m}}$  with crack region masked in blue

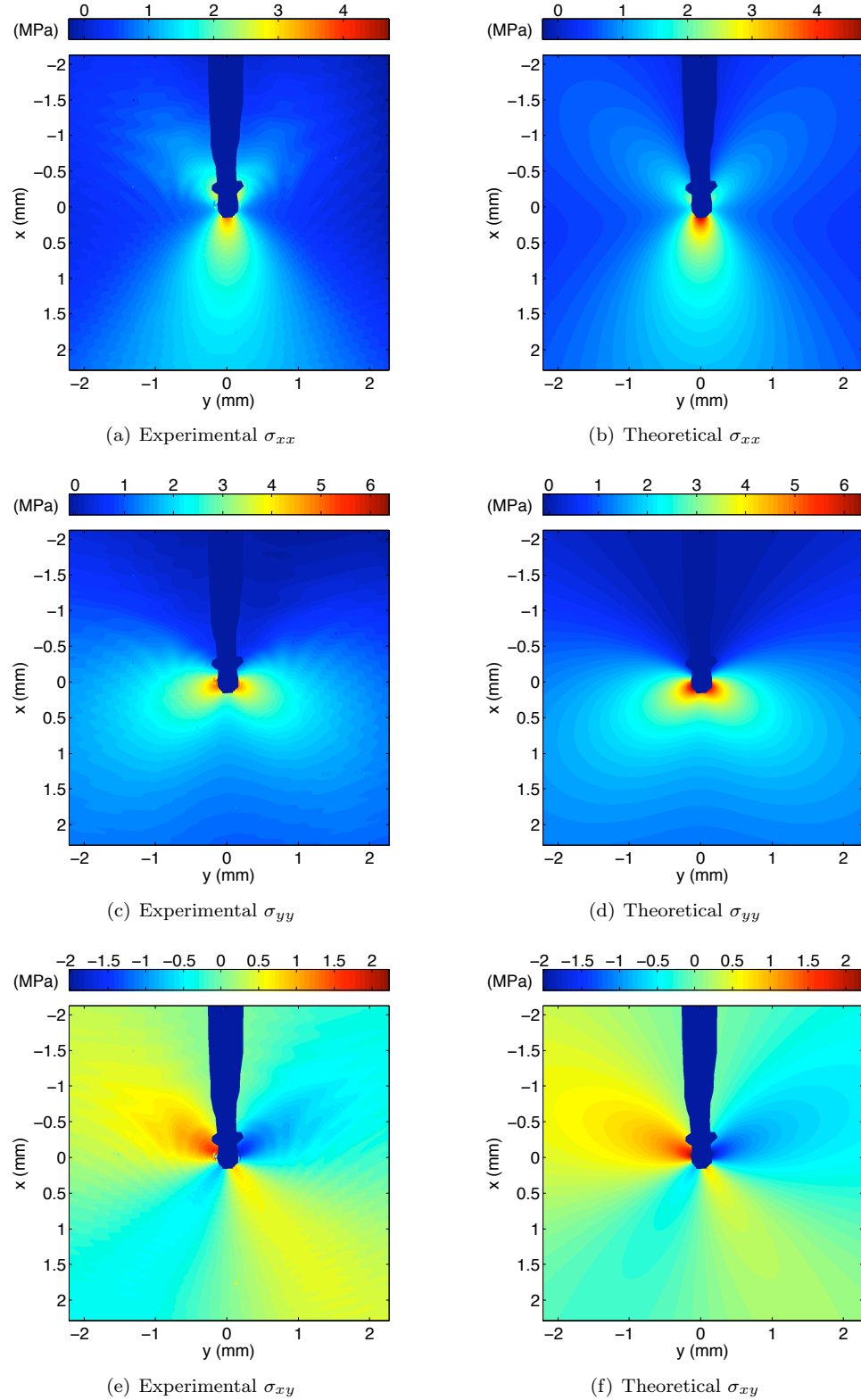


Figure 4.54: Experimental and theoretical data for the Cartesian stresses for specimen HomC2 for  $K_I = 0.145 \text{ MPa}\sqrt{\text{m}}$  and  $K_{II} = 0.63 \text{ kPa}\sqrt{\text{m}}$  with crack region masked in blue

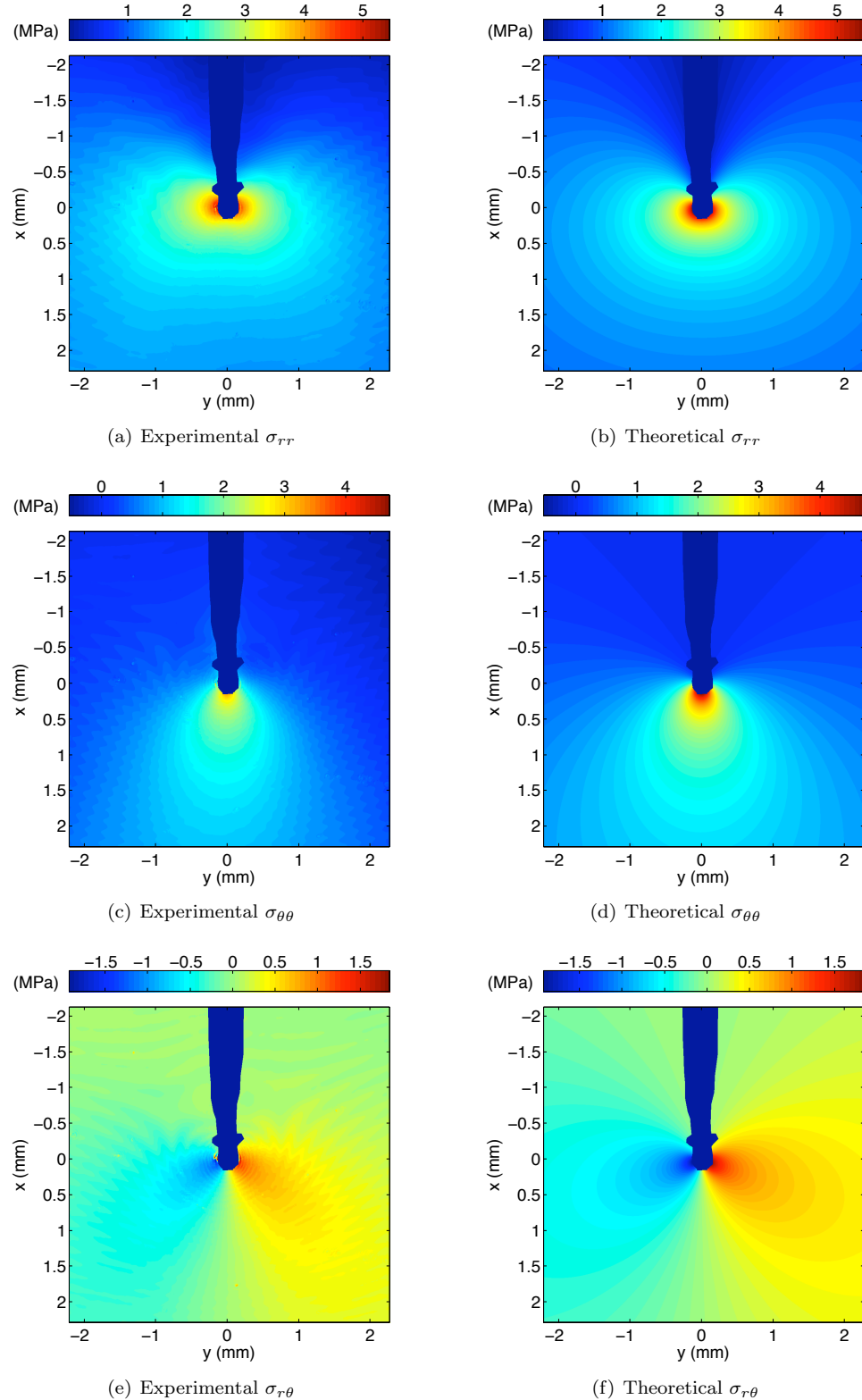


Figure 4.55: Experimental and theoretical data for the polar stresses for specimen HomC2 for  $K_I = 0.145 \text{ MPa}\sqrt{\text{m}}$  and  $K_{II} = 0.63 \text{ kPa}\sqrt{\text{m}}$  with crack region masked in blue

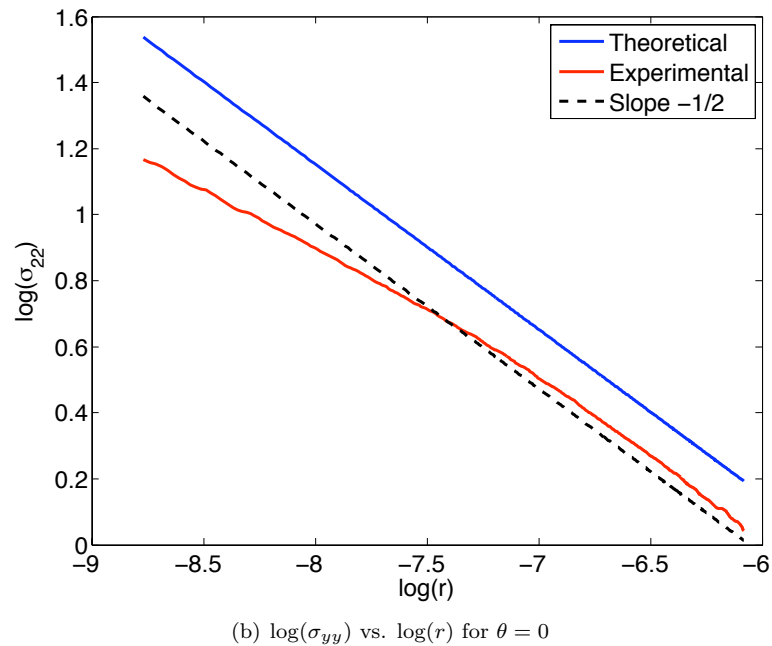
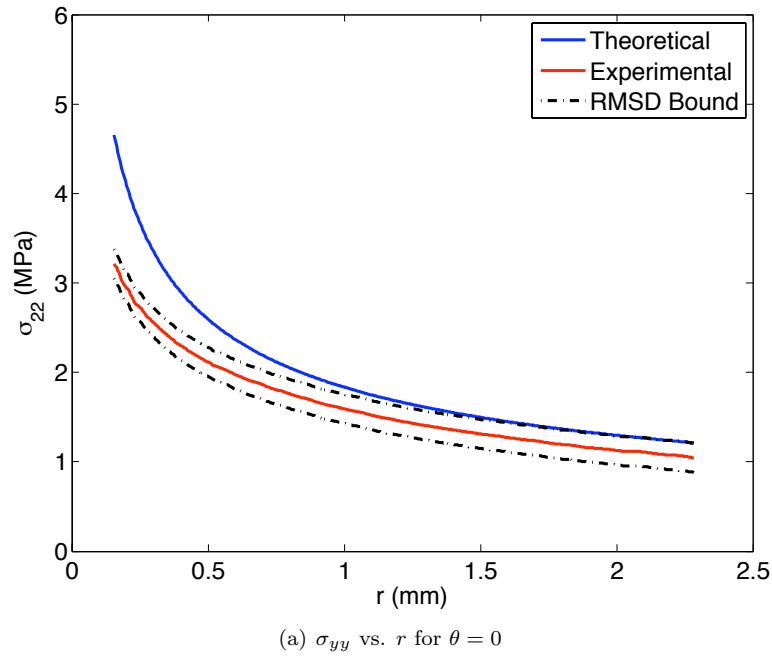


Figure 4.56: Experimental and theoretical data for  $\sigma_{yy}$  along  $\theta = 0$  for specimen HomC2 for  $K_I = 0.145 \text{ MPa}\sqrt{\text{m}}$  and  $K_{II} = 0.63 \text{ kPa}\sqrt{\text{m}}$ : The experimental data is slightly lower than the theoretical data, but with similar  $r^{-1/2}$  dependence seen by the near  $-1/2$  slope on the log-log plot of  $\sigma_{yy}$  versus  $r$ .